Specific binding of Hsp27 and phosphorylated Tau mitigates abnormal Tau aggregation-induced pathology

Shengnan Zhang[1¶], Yi Zhu[2¶], Jinxia Lu[3 ¶], Zhenying Liu[1,4¶], Amanda G. Lobato[2,5], Jiaqi Liu[2,6], Jiali Qiang[1], Wen Zeng[1,4], Yaoyang Zhang[1], Cong Liu[1], Zhuohao He[1], R. Grace Zhai[2]*, Dan Li[3]*

[1] Interdisciplinary Research Center on Biology and Chemistry, Shanghai Institute of Organic Chemistry, Chinese Academy of Sciences, 100 Haike Road, Shanghai 201210, China;

[2]Department of Molecular and Cellular Pharmacology, University of Miami Miller School of Medicine, Miami, FL 33136, USA;

[3]Bio-X Institutes, Key Laboratory for the Genetics of Developmental and Neuropsychiatric Disorders (Ministry of Education), Shanghai Jiao Tong University, Shanghai, China;

[4]University of the Chinese Academy of Sciences, 19 A Yuquan Road, Shijingshan District, Beijing 100049, China;

[5]Graduate Program in Human Genetics and Genomics, University of Miami Miller School of Medicine, Miami, FL 33136, USA.

[6]Graduate Program in Molecular and Cellular Pharmacology, University of Miami Miller School of Medicine, Miami, FL 33136, USA.

¶These authors contributed equally to this work.

*To whom correspondence should be addressed. E-mails: lidan2017@sjtu.edu.cn, and gzhai@med.miami.edu

Abstract

Amyloid aggregation of phosphorylated Tau (pTau) into neurofibrillary tangles is closely associated with Alzheimer's disease (AD). Several molecular chaperones have been reported to bind Tau and impede its pathological aggregation. Recent findings of elevated levels of Hsp27 in the brains of patients with AD suggested its important role in pTau pathology. However, the molecular mechanism of Hsp27 in pTau aggregation remains poorly understood. Here, we show that Hsp27 partially co-localizes with pTau tangles in the brains of patients with AD. Notably, phosphorylation of Tau by microtubule affinity regulating kinase 2 (MARK2), dramatically enhances the binding affinity of Hsp27 to Tau. Moreover, Hsp27 efficiently prevents pTau fibrillation *in vitro* and mitigates neuropathology of pTau aggregation in a *Drosophila* tauopathy model. Further mechanistic study reveals that Hsp27 employs its N-terminal domain to directly interact with multiple phosphorylation sites of pTau for specific binding. Our work provides the structural basis for the specific recognition of Hsp27 to pathogenic pTau, and highlights the important role of Hsp27 in preventing abnormal aggregation and pathology of pTau in AD.

Keywords:

Hsp27; Alzheimer's disease; tauopathy; phosphorylated Tau; chaperone;

Introduction

Pathological aggregation and propagation of microtubule-associated protein Tau is closely associated with Alzheimer's disease (AD), frontotemporal dementia (FTD), and other tauopathies (Avila, 2006; Hanger et al., 2009; Hanger et al., 1998; Hanger et al., 1991; Spillantini and Goedert, 2013). Tau is hyper-phosphorylated and forms amyloid fibrils in neurofibrillary tangles (NFT) in patients' brains which is the pathological hallmark of AD. Tau is abundant in the axons of neurons where it stabilizes microtubules (MT) (Drechsel et al., 1992; Drubin and Kirschner, 1986). Under diseased conditions, abnormal phosphorylation of Tau in the regions surrounding the microtubule-binding domain by kinases such as microtubule affinity regulating kinase (MARK) and glycogen synthase kinase 3 (GSK3) leads to dissociation of Tau from MT and subsequent pathological aggregation (Ando et al., 2016; Biernat et al., 1993; Drewes, 2004; Drewes et al., 1997; Hanger et al., 2009; Martin et al., 2013). Moreover, the amyloid fibrils formed by phosphorylated Tau (pTau) have been found to be more potent to mediate the propagation and spread of Tau pathology than those formed by unphosphorylated Tau (Dujardin et al., 2020; Hu et al., 2016; Rosenqvist et al., 2018). Pathological pTau fibrils have been extracted from AD brains, and Hsp27 has been found to co-precipitate with them (Shimura et al., 2004). This suggests that Hsp27 may play an important role in pTau pathology.

Hsp27 is a member of the small heat shock protein (sHsp) family which participates in the cellular chaperone network to maintain protein homeostasis by preventing protein abnormal aggregation (Haslbeck et al., 2005). It is ubiquitously expressed and plays a protective role in a variety of cellular processes (Jakob et al., 1993). Emerging pieces of evidence suggest the importance of Hsp27 in AD and other tauopathies. For instance, the expression level of Hsp27 is significantly elevated in affected brain tissues of patients with AD (Bjorkdahl et al., 2008; Renkawek et al., 1994), as well as patients with other tauopathies including progressive supranuclear palsy (PSP) and corticobasal degeneration (CBD) (Schwarz et al., 2010). Moreover, Hsp27 can effectively inhibit the amyloid aggregation of unphosphorylated Tau *in vitro* (Baughman et al., 2018; Baughman et al., 2020; Freilich et al., 2018), prevent cellular toxicity of Tau in SH-

SY5Y cells (Choi et al., 2015), and rescue tauopathies in Tau transgenic mice (Abisambra et al., 2010). However, the molecular mechanism of the interplay between Hsp27 and pTau, which exhibits more pathological relevance than that between Hsp27 and unphosphorylated Tau, remains poorly understood.

In this study, we first examined the post-mortem brain tissue of patients with AD and detected the co-localization of Hsp27 and pTau aggregates. We next took advantage of a *Drosophila* tauopathy model and uncovered the neuroprotective effects of Hsp27 against pTau-induced synaptopathy *in vivo*. To dissect the molecular mechanism, we characterized the interaction between Hsp27 and MARK2-mediated hyper-phosphorylated pTau,y and the consequent amyloid aggregation *in vitro*. Employing multiple biophysical and computational approaches, we revealed that Hsp27 recognizes multiple phosphorylation sites of pTau to prevent pTau amyloid aggregation. This work provides molecular insights into the important role of Hsp27 in preventing pTau pathology in AD.

Results

Co-localization of Hsp27 and Tau pathology in human brains with AD

We first asked whether Hsp27 is associated with pathological pTau aggregates in AD brains. We obtained human frontal cortex tissue slices from two cases of AD patients and two cases of age-matched healthy controls (Table 1). Immunofluorescence staining using antibodies anti-pTau^{Ser262} and anti-Hsp27 detected the presence of pTau in two AD cases, but absent in two healthy controls (Figure 1). Notably, Hsp27 was detected at a high level in AD brain slices, but at a much lower or undetectable level in healthy control brain slices (Figure1), consistent with previous findings of elevated Hsp27 levels in AD brains (Bjorkdahl et al., 2008; Renkawek et al., 1994). More importantly, Hsp27 was found to co-localize with the pTau aggregates in both AD cases (Figure1), suggesting the pathological relevance between Hsp27 and pTau pathology in AD. Note that not all pTau aggregates contain Hsp27 and vice versa, especially in case 1, which may reflect the heterogeneity of the protein aggregates.

Hsp27 protects pTau-induced synaptopathy in *Drosophila*

To investigate the influence of Hsp27 on the abnormal aggregation of pTau and its neuropathology *in vivo*, we used a *Drosophila* tauopathy model where human pathogenic mutant Tau (Tau^{R406W}), associated with FTD with parkinsonism linked to chromosome 17 (FTDP-17), is expressed in the nervous system by a pan-neuronal driver *elav^{C155}-GAL4*. Our previous work has demonstrated that the expression of human Tau^{R406W} in the *Drosophila* nervous system leads to age-dependent neurodegeneration recapitulating some of the salient features of tauopathy in FTDP-17 (Ali et al., 2012; Ma et al., 2020). To quantitatively assess the pTau species in the brain, we carried out western blot analysis using a total Tau antibody 5A6 (Johnson et al., 1997), a $pTau^{Ser262}$ specific antibody (Iijima et al., 2010), and a hyper-phosphorylated Tau antibody AT8 that recognizes hyper-phosphorylation at Ser202 and Thr205 sites (Goedert et al., 1995). As shown in Figure 2A and B, Hsp27 overexpression significantly reduced the level of hyper-phosphorylated Tau at both 2 and 10 days after eclosion (DAE).

We next examined the morphology of the fly brain as well as the accumulation of hyper-phosphorylated Tau by immunofluorescence staining. In these analyses, we used the AT8 antibody to label hyper-phosphorylated Tau because phosphorylation at Ser202 and Thr205 occurs after the phosphorylation of S262 and is associated with advanced pathology (Wesseling et al., 2020). Consistent with previous findings, brains with neuronal expression of Tau^{R406W} exhibited an accumulation of filamentous pTau and a reduction of brain neuropil size indicative of neurodegeneration (Figure 2C-F). Interestingly, we found that neuronal expression of Tau^{R406W} led to a significant upregulation of endogenous Hsp27, which was highly enriched in the synaptic areas (Figure 2C and D), suggesting that Hsp27 might be a part of the neuronal stress response network that is upregulated upon proteotoxic stress. Importantly, overexpression of Hsp27 restored the size of brain neuropil and suppressed the accumulation of filamentous pTau (Figure 2C-F), suggesting that Hsp27 protects against mutant Tau^{R406W} induced neurodegeneration.

Synaptic loss is a hallmark of human tauopathy (McGowan et al., 2006). To evaluate the synaptic integrity, we took advantage of the *Drosophila* visual system with highly organized paralleled photoreceptor structures (Fischbach and Dittrich, 1989). We have previously shown that Tau^{R406W} expression resulted in synaptic aggregation of hyper-phosphorylated Tau as well as a significant reduction of Bruchpilot (Brp), an active zone associated-cytoskeletal matrix protein, at lamina cartridge, suggesting a severe loss of the active zone structures in the presynaptic terminals (Ma et al., 2020). As shown in Figure 2G-I, we expressed Tau^{R406W} with either GFP (control) or Hsp27 in the photoreceptors using *GMR-GAL4* and found that overexpression of Hsp27 led to a remarkable reduction of synaptic pTau and enhanced BRP localization, indicating a restoration of synaptic integrity.

Taken together, we showed that Hsp27 protects against synaptic dysfunction in a *Drosophila* tauopathy model by reducing pTau aggregation and ameliorating pTau-induced synaptic degeneration.

Hsp27 specifically binds pTau and prevents its amyloid aggregation

We next sought to examine the binding of Hsp27 with pTau and its effect on pTau amyloid aggregation *in vitro*. We purified the longest Tau isoform – Tau40 that contains both the projection region and four microtubule-binding repeat domains (R1–R4), as well as K19, a truncated Tau construct that contains R1, R3, and R4 (Figure 3A). Then phosphorylated Tau, including pTau40 and pK19, were prepared by phosphorylating purified Tau40 and K19 using kinase MARK2 which was previously identified to be important in mediating pTau pathology in AD (Ando et al., 2016; Drewes, 2004; Gu et al., 2013). Two dimensional (2D) ^{1}H-^{15}N HSQC spectra enable us to monitor each of the MARK2 phosphorylation sites in both pTau40 and pK19. Consistent with previous report (Schwalbe et al., 2013), eight MARK2 phosphorylation sites including pS262, pS293, pS305, pS324, pS352, pS356, pS413 and pS416 were identified on the HSQC spectrum of pTau40 (Figure supplementary 1A). Four phosphorylation sites including pS262, pS324, pS352, and pS356 were identified on the HSQC spectrum of pK19 (Figure supplementary 1B). Most of these phosphorylation sites are within the fibril

forming core region of Tau, and two of them including pS262 and pS356 have been widely reported to be essential for the detachment of pTau from MT and cause increased toxicity in animal models (3, 4, 28).

We used BioLayer Interferometry (BLI) assay to measure the binding affinity of Hsp27 with pTau and unphosphorylated Tau, respectively. pTau and Tau were immobilized on biosensor tips, and the association and dissociation curves were measured in the presence and absence of various concentrations of Hsp27 to calculate the equilibrium dissociation constant (K_D) between Hsp27 and pTau/Tau. Notably, the K_D value of Hsp27/pTau40 is ~ 1.61 μM (Figure 3B). The K_D value for Hsp27/pK19 is ~ 1.99 μM (Figure 3C) which is similar to that of Hsp27/pTau40, suggesting that pK19 serves as the key region for binding of Hsp27 to pTau40. In sharp comparison, the binding of both Hsp27/Tau40 and Hsp27/K19 were much weaker which cannot be detectable under our experimental condition (Figure 3B and C). These results demonstrate that hyper-phosphorylation significantly enhances the binding of Hsp27 to both pTau40 and pK19.

We further assessed the influence of Hsp27 on the amyloid aggregation of pTau40 and pK19 by thioflavin T (ThT) fluorescence assay and negative-staining electron microscopy (EM). The results showed that Hsp27 effectively inhibited the amyloid aggregation of both pTau40 and pK19 in a dose-dependent manner (Figure 3D and E). Together, our data show that Hsp27 can specifically bind to hyper-phosphorylated Tau including pTau40 and pK19, and efficiently prevent their amyloid aggregation.

Hsp27 directly binds to multiple phosphorylation sites of pTau

To investigate the structural basis of the interaction between Hsp27 and pTau, we performed solution NMR spectroscopy, and titrated Hsp27 to ^{15}N-labeled pTau40 and ^{15}N-labeled pK19, respectively. Strikingly, the 2D ^{1}H-^{15}N HSQC spectra showed obvious chemical shift changes (CSDs) of all the eight phosphorylated Ser (pSer) residues of pTau40 and four pSer residues of pK19 upon titration of Hsp27 (Figure 4A and B). The highly overlapped signals in the pTau40 HSQC spectrum exclude us to obtain a full assignment of pTau40. Alternatively, we accomplished the backbone

assignment of pK19, which enables us to map the binding interface of pK19 with Hsp27. As shown in Figure 3C, the regions containing the four pSer residues of pK19 harbor prominent CSDs. Among them, the two pSer residues in R4 showed the largest CSDs above 0.06 ppm (Figure 4C). In addition, titration of Hsp27 to pK19 induced dramatically intensity drops of most residues of pK19 (Figure 4C), implying the direct binding of Hsp27 to pK19 which increases the molecular weight upon pK19-Hsp27 complex formation, and thus increases line width of the cross peaks. By contrast, addition of the same amount of Hsp27 to unphosphorylated Tau including Tau40 and K19 only results in slightly CSD and intensity perturbations (Figure supplementary 2). Together, our data suggest that phosphorylation of Tau promotes the interaction between Hsp27 and pTau by forming the specific interaction between Hsp27 and the phosphorylated residues of Tau.

N-terminal domain (NTD) of Hsp27 mediates the binding of Hsp27 to pTau

Hsp27 composes of a central α-crystallin domain (ACD) flanked by a flexible NTD and a flexible C-terminal domain (CTD). To further dissect the role of different domains of Hsp27 in binding pK19, four different truncations of Hsp27 were prepared (Figure 5A). Their binding affinities to pK19 were determined by BLI, respectively. Notably, the isolated NTD binds to pK19 with a K_D value of ~ 0.57 μM which is similar to the binding affinity of the full-length Hsp27 to pK19 (Figure 5B). ΔCTD which contains both NTD and ACD display a similar binding affinity to pK19 (0.67 ± 0.01 μM) (Figure 5B). In contrast, both ACD and ΔNTD which do not contain NTD show no detectable binding to pK19 at the same condition (Figure 5C and Figure supplementary 3). Together, these data suggest that Hsp27 NTD plays an essential role in mediating the binding of Hsp27 to pK19.

Next, we performed cross-linking mass spectrometry (CL-MS) to map the interacting regions of Hsp27 and pK19. NTD of Hsp27 contains 0 lysine residue. Whereas, negatively charged residues including glutamine acid (E) and aspartic acid (D) evenly distribute within the three different domains of Hsp27 (Figure 5D). Thus, we performed a two-step coupling procedure using cross-linkers 1-ethyl-3-(3-

dimethylaminopropyl) carbodiimide (EDC) and sulfo-N-hydroxysulfosuccinimide (sulfo-NHS) to crosslink Hsp27 and pK19. EDC causes direct conjugation of carboxylates (-COOH) to primary amines ($-NH_2$) of target molecules, and sulfo-NHS is introduced for stabilization. We identified two pairs of cross-linked segments between Hsp27 and pK19 with a confidence score of $<10^{-6}$ by mass spectrometry, including $E3_{Hsp27}$-$K331_{pK19}$ and $D30_{Hsp27}$-$K311_{pK19}$ (Figure 5D, 5E and Table 2). Notably, both cross-linked segments are formed by residues located at R3 of pK19 and NTD of Hsp27 (Figure 5D), which is consistent with our NMR titration that residues at R3 show slightly stronger intensity drop upon addition of Hsp27, and the domain truncation mapping results. Together, our data demonstrate that NTD is essential to mediate pK19 binding.

Different domains of Hsp27 bind distinct regions of pK19 to prevent its fibrillation

To further pinpoint the binding regions of pK19 by NTD and other domains of Hsp27, we titrated full-length and the four truncations of Hsp27 to ^{15}N-labeled pK19 and collected a series of HSQC spectra. As shown in Figure 6A and B, titration of both NTD and ΔCTD induce significant CSDs mainly located on the four pSer sites of pK19, which recapitulates that titrated by full-length Hsp27. In contrast, titration of ACD or ΔNTD caused much smaller CSDs on the four pSer sites of pK19. Moreover, addition of NTD and ΔCTD induces overall intensity drops of pK19 signals (~ $I/I_0 < 0.8$), while titration of ACD and ΔNTD only cause slightly intensity drops. These results demonstrate that Hsp27 mainly uses its NTD to directly interact with the pSer residues of pK19 for pTau binding, which is consistent with the BLI results.

Notably, we found that despite that titration of ACD doesn't induce CSDs of the pSer sites, it causes relative small but detectable CSDs (> 0.01 ppm) and intensity drops ($I/I_0 < 0.7$) of the highly amyloidogenic region - ^{306}VQIVYK^{311} of pK19, especially residues V309、Y310 and K311 (Figure 6A and 6B). This demonstrates that ACD is capable of directly binding to pK19 via its VQIVYK region. Of note, the cross peaks of V306, Q307, and I308 severely overlapped with a few residues of pK19 which excludes us to obtain the accurate CSD and intensity changes upon titration.

Together, our results demonstrate that different domains of Hsp27 display distinct binding preferences to different regions of pK19. NTD exhibits a high binding affinity to the multiple pSer sites of pK19, while ACD weakly binds the amyloidogenic VQIVYK segment of pK19.

Finally, we examined the role of different domains of Hsp27 in preventing amyloid aggregation of pK19 and pTau40. As shown in Figure 7A and B, NTD-containing Hsp27 variants including full-length Hsp27, ΔCTD, and NTD exhibits potent inhibitory activity in preventing both pTau40 and pK19 fibrillation. This suggests that strong binding of NTD to the phosphorylated sites of pTau is important in preventing pTau fibrillation. Interestingly, ACD and ΔNTD display weakened but not negligible inhibitory activity of pTau, especially for pK19. This suggests that binding of ACD to the VQIVYK segment of pTau may result in moderate inhibition of pTau fibrillation. Together, our data show that the NTD is predominately employed to bind pTau to prevent its fibrillation, while ACD also contributes chaperone activity to a less degree by binding to the highly aggregation-prone VQIVYK region of pTau.

Discussion

Molecular chaperones play essential roles in maintaining protein homeostasis and preventing protein misfolding and aggregation. Accumulating evidence showed that many molecular chaperones including Hsp70, DnaJA2, Hsp90, Hsp27, and NMNAT can directly interact with Tau and are involved in different steps of Tau biogenesis, aggregation, and clearance (Baughman et al., 2018; Freilich et al., 2018; Ma et al., 2020; Mok et al., 2018; Petrucelli et al., 2004). Since Hsp27 was identified to co-precipitate with AD brain-derived pTau aggregates and is elevated in AD brains (Bjorkdahl et al., 2008; Renkawek et al., 1994; Shimura et al., 2004), Hsp27 may play an important role in interacting with pTau in AD. Indeed, we showed elevated Hsp27 levels and partial co-localization of Hsp27 with pTau aggregates in AD brains. More importantly, we found that MARK2-mediated phosphorylation of Tau dramatically increases the binding of pTau to Hsp27, strengthening the notion that Hsp27 binds specifically to

disease-related pTau. This specific binding enables Hsp27 to be a potent chaperone in inhibiting amyloid aggregation of MARK2-mediated phosphorylated Tau *in vitro*.

Over 58 different phosphorylation sites including MARK2-phosphorylation sites were identified on Tau40 in AD brains (Hanger et al., 1998; Hanger et al., 2007; Hasegawa et al., 1992; Morishima-Kawashima et al., 1995; Wesseling et al., 2020; Xia et al., 2021). Phosphorylation at different sites is believed to be involved in different stages of pTau pathology in AD (Hanger et al., 2009; Wesseling et al., 2020; Xia et al., 2021). A previous study examined the inhibitory activity of different chaperons to unmodified Tau and Tau carrying single-point mutations at different phosphorylation sites including S356E, T153E, T231E, S396E, and S404E (Mok et al., 2018). Among them, only S356 belongs to MARK2-phosphorylation sites (Figure 4A). Strikingly, Hsp27 exhibits potent inhibitory activity on S356E Tau but not the other Tau phosphomimetics (Mok et al., 2018). This suggests the binding specificity of Hsp27 on different phosphorylation sites of Tau. It will be important to further explore whether Hsp27 recognizes the other disease-related phosphorylation sites in addition to those modified by MARK2. Moreover, other molecular chaperones including Hsp90 and NMNAT were also found to mediate pTau cellular clearance and prevent pTau aggregation both *in vitro* and in cells (Dickey et al., 2007; Ma et al., 2020). The important questions that remained to be addressed include: (1) whether different chaperones preferentially recognize Tau with different phosphorylation patterns; (2) how different chaperones coordinate to prevent disease-related pTau aggregation and pathology.

Hsp27 contains three domains including NTD, ACD, and CTD. We showed in this study that Hsp27 uses its NTD to strongly bind to the multiple phosphorylation sites of pTau. Meanwhile, ACD of Hsp27 transiently and weakly interacts with the highly amyloidogenic region - ^{306}VQIVYK^{311} of pTau. Therefore, different domains of Hsp27 are responsible for binding to distinct regions of pTau. Notably, previous studies showed that, as for the unphosphorylated Tau, ACD exhibits the strongest binding ability by predominantly binding the ^{306}VQIVYK^{311} region of Tau via its β4 and β8

region (Baughman et al., 2018; Baughman et al., 2020; Freilich et al., 2018). While NTD displays much weaker binding to unmodified Tau (Baughman et al., 2020; Freilich et al., 2018). Therefore, phosphorylation of Tau shifts the paradigm of Hsp27 binding pattern of Tau, which results in significantly enhanced overall binding of Hsp27 to pTau. As the phosphorylation pattern of pTau is dynamically changed upon the progression of AD (Hanger et al., 2009; Wesseling et al., 2020; Xia et al., 2021), how phosphorylation at different sites influences the interplay between pTau and its binding patterns including Hsp27 and different molecular chaperones will be interesting to investigate.

This study demonstrates that NTD of Hsp27 is essential for binding to the phosphorylation sites of pTau. Notably, Hsp27 was found to be phosphorylated at multiple sites on NTD under stress conditions, which leads to dissociation of Hsp27 from high-molecular-weight oligomers to smaller ones with higher chaperone activities (Alderson et al., 2019; Jovcevski et al., 2017; Jovcevski et al., 2015; Lambert et al., 1999; Rogalla et al., 1999). Our previous work showed that NTD phosphorylation provides an additional layer for regulating Hsp27 activity in controlling the phase separation and amyloid fibrillation of ALS-associated FUS (Liu et al., 2020). Whether Hsp27 NTD is phosphorylated under the disease conditions of AD, FTD, and other tauopathies, and how Hsp27 NTD phosphorylation influences the binding and chaperone activity of Hsp27 to pTau are both worthy of being further explored to fully appreciate the complicated interplay between pTau and Hsp27 in disease. Nevertheless, our study demonstrates the important role of Hsp27 in chaperoning pathological pTau from abnormal aggregation, and implies that activating Hsp27 or elevating its level might be a potential strategy for AD treatment.

Material and Methods

Human brain samples and immunofluorescence

Human brain samples were originally from the tissue bank of the Center for Neurodegenerative Disease Research (CNDR) at the University of Pennsylvania. 10% neutral buffered formalin (NBF)-fixed, paraffin-embedded human frontal cortex tissues

from two AD patients and two age-matched normal controls were sectioned into 6 μm slices, and immunostained as described before (He et al., 2018). Briefly, after deparaffinization and rehydration, the brain slices were incubated with anti-human Hsp27 (1:200, Cat. # ab2790) and anti-pTau^{Ser262} (1:200, Cat.# ab131354) antibodies overnight at 4 °C followed by a 2-h incubation of Alexa Fluor-conjugated secondary antibodies (Thermo Fisher Scientific), and then mounted with DAPI-containing Fluoromount-G (SouthernBiotech, USA).

Drosophila stocks and genetics

The following fly strains were used: *UAS-Hsp27* (generated in this study); *UAS-Tau^{R406W}* obtained from Dr. Mel Feany (Wittmann et al., 2001); *yw*, *UAS-GFP*, *elav-GAL4*, *GMR-GAL4* obtained from Bloomington Drosophila Stock Center. Flies were reared at 25 °C with 65% humidity, 12 h light/12 h dark cycles.

Western blot

For protein extraction in flies, ten heads of each group were homogenized in radioimmunoprecipitation assay (RIPA) buffer (Sigma-Aldrich, R0278). Samples were mixed with Laemmli sample buffer containing 2% SDS, 10% glycerol, 62.5 mM Tris-HCl (pH 6.8), 0.001% bromophenol blue, and 5% β-mercaptoethanol, and heated at 95 °C for 10 mins. Proteins were separated by SDS-polyacrylamide gel electrophoresis and transferred to a nitrocellulose membrane. After blocking at room temperature for 1.5 h, the membrane was incubated with primary antibody at 4 °C overnight, followed by secondary antibody for 1.5 h at room temperature. Imaging was performed on an Odyssey Infrared Imaging system (LI-COR Biosciences) and analyzed using Image Studio (ver 4.0). Primary antibody dilutions were used as follows: anti-pTau$^{Ser202/Thr205}$ (AT8, 1:500; ThermoScientific, Rockford, IL, USA), anti-pTau^{Ser262} (1:1000; ThermoScientific), anti-β-actin (1:5000, Sigma-Aldrich, St Louis, MO, USA), anti-total-Tau (5A6, 1:250, Developmental Studies Hybridoma Bank, Iowa City, IA, USA).

Fly brain dissection, immunostaining, and confocal microscopy

Fly brains were dissected in phosphate-buffered saline (PBS, pH 7.4) and fixed with 4% formaldehyde at room temperature for 10 mins. After 10 mins washing in PBTx (PBS containing 0.4% v/v Triton X-100) 3 times, brains were incubated with primary antibodies diluted in PBTx with 5% normal goat serum at 4 °C overnight. Fly brains were incubated with conjugated secondary antibodies at room temperature for 1 h, followed by 4',6- diamidino-2-phenylindole (DAPI, 1:300, Invitrogen, Carlsbad, CA, USA) staining for 15 mins. Brains were mounted on slides with VECTASHIELD Antifade Mounting Medium (Vector Laboratories Inc., Burlingame, CA, USA). After that, brains were imaged using an Olympus IX81 confocal microscope coupled with a 60× oil immersion objective lens with a scan speed of 8.0 µs per pixel and spatial resolution of 1024 × 1024 pixels. Images were processed using FluoView 10-ASW (Olympus) and Adobe Photoshop CS6 and quantified using Fiji/Image J (ver 1.52). Primary antibody dilutions were used as follows: anti-pTau$^{Ser202/Thr205}$ (AT8, 1:250), anti-BRP (nc82, 1:250, Developmental Studies Hybridoma Bank), anti-Hsp27 (1:250, Abcam, Cambridge, MA, USA).

Plasmid construction for *in vitro* study.

Genes of full-length human Hsp27 (UniProt accession number P04792), and the truncations of Hsp27 including NTD (residues of 1-84), ΔCTD (residues of 1-176), ΔNTD (residues of 85-205), and ACD (residues of 85-175) were inserted into a pET-28a vector with an N-terminal His_6-tag and a following tobacco etch virus (TEV) protease cleavage site. Sequencing of all constructs was verified by GENEWIZ company (Suzhou, China).

Protein expression and purification

All proteins were expressed in *Escherichia coli* BL21(DE3) cells, grown to an OD_{600} of 0.8 and induced with 0.3 mM IPTG overnight at 16 °C. Hsp27 and its variants were purified with HisTrap^{TM}FF column (GE Healthcare) with the Tris buffer (50 mM Tris-HCl, 100 mM NaCl, a gradient of 0~500 mM imidazole, pH 8.0). The N-terminal His_6-tag and Trx1-tag were removed using TEV protease in the buffer of 50 mM Tris-HCl, 100 mM NaCl, pH 8.0. The cleaved proteins were immediately loaded onto the size-exclusion chromatography column Superdex 75 26/60 (GE Healthcare) with a PBS buffer of 50 mM sodium phosphate, 50 mM NaCl at pH 7.0.

Human Tau40 and K19 were over-expressed and purified as previously described (Barghorn et al., 2005). Briefly, Tau/K19 was purified by a HighTrap HP SP (5 ml) column (GE Healthcare), and followed by a Superdex 75 gel filtration column (GE Healthcare).

For ^{15}N-labeled proteins, protein expression was the same as that for unlabeled proteins except that the cells were grown in M9 minimal medium with $^{15}NH_4Cl$ (1 g l^{-1}). Purification of ^{15}N-labeled proteins was the same as that of the unlabeled proteins.

The purity of proteins was assessed by SDS-PAGE. Protein concentration was determined by BCA assay (Thermo Fisher).

In vitro phosphorylation of Tau40/K19

Phosphorylation of Tau40/K19 by MARK2 kinase was carried out following a method described previously (Ma et al., 2020). Briefly, Tau40/K19 was incubated with cat MARK2-T208E at a molar ratio of 10:1 in a buffer of 50 mM Hepes, pH 8.0, 150 mM

KCl, 10 mM $MgCl_2$, 5 mM ethylene glycol tetraacetic acid (EGTA), 1 mM PMSF, 1 mM dithio-threitol (DTT), 2 mM ATP (Sigma), and protease inhibitor cocktail (Roche) at 30 °C overnight. pTau40/pK19 was further purified by HPLC (Agilent) to remove kinase, and lyophilized. The sites and degrees of phosphorylation were quantified using 2D ^{1}H-^{15}N HSQC spectrum according to previous publications (Schwalbe et al., 2013).

NMR spectroscopy

All NMR experiments were performed at 298 K in the NMR buffer of 50 mM sodium phosphate, 50 mM NaCl, and 10% (v/v) D_2O at pH 7.0. 3D HNCA and HNCACB experiments were collected on an Agilent 600 MHz spectrometer for backbone assignment of K19, while 3D HNCA, HNCOCA, CBCACONH, and HNCACB experiments were collected for backbone assignment of pK19. NMR titrations were performed on a Bruker 900 M or Agilent 800 MHz spectrometer. Each sample (500 µl) was made of 50 µM ^{15}N-pTau40/pK19/Tau40/K19, in the absence or presence of Hsp27 and its variants at the indicated concentrations. Intensity changes were calculated by I/I_0. And chemical shift deviations (CSDs, Δδ) were calculated using equation,

$$\Delta\delta = \sqrt{(\Delta\delta 1\mathrm{H})^2 + 0.0289(\Delta\delta 15\mathrm{N})^2}$$

Where Δδ1H and Δδ15N are the chemical shift differences of amide proton and amide nitrogen between free and bound state of the protein, respectively. All NMR spectra were processed using NMRPipe (F et al., 1995) and analyzed using Sparky (Lee et al., 2015) and NMRView (Johnson, 2004).

BioLayer Interferometry (BLI) assay

The binding kinetics of the Tau proteins to Hsp27 WT and variants were measured by BLI on an ForteBio Octet RED96 system (Pall ForteBio LLC). Experiments were performed at room temperature using the assay buffer of 50 mM sodium phosphate, 50 mM NaCl, pH 7.0. Tau proteins including pTau40, Tau40, pK19, and K19 were firstly biotinylated by incubating 0.5-1 mg/ml proteins with biotin at a molar ratio of protein: biotin of 2:3 at 4 °C for 30 mins, then the excess biotins were removed by desalting column (Zeba Spin Desalting Columns, Thermo). Then biotinylated Tau proteins were immobilized onto streptavidin biosensors (ForteBio) individually, and incubated with varying concentrations of Hsp27 WT and variants as indicated in the figure. The kinetic experiments were performed following the protocol previously (Zhang et al., 2021), in which an auto-inhibition step was used to eliminate the non-specifically binding of Hsp27 and its variants to biosensors. The resulting curves were corrected using the blank reference and analyzed by the ForteBio Data Analysis software 9.0.

ThT fluorescence assay

ThT kinetics of pTau/pK19 in the absence and presence of Hsp27 and its variants were recorded using a Varioskan Flash Spectral Scanning Multimode Reader (Thermo Fisher Scientific) with sealed 384-microwell plates (Greiner Bio-One). The assay buffer is 30mM PBS, 2 mM $MgCl_2$, 1 mM DTT, 0.05% NaN_3, pH 7.4. 0.5% (v/v) of fibril seeds (the seeds were prepared by sonicating fibrils for 15 s) were added to promote the fibril formation of pTau/pK19. ThT fluorescence with a final ThT concentration of 30 μM in each sample was measured in triplicates with shaking at 600 *rpm* at 37 °C with excitation at 440 nm and emission at 485 nm.

Transmission electron microscopy (TEM)

5 μl of samples were applied to fresh glow-discharged 300-mesh copper carbon grids and stained with 3% v/v uranyl acetate. Specimens were examined by using Tecnai G2 Spirit TEM operated at an accelerating voltage of 120 kV. Images were recorded using a 4K × 4K charge-coupled device camera (BM-Eagle, FEI Tecnai).

Cross-linking mass spectrometry analysis

Cross-linking experiments were modified from the protocol previously (Zhou et al., 2015). 0.4 mg EDC (final concentration of ~2 mM) and 1.1 mg Sulfo-NHS (final concentration of ~5 mM) were added to 1 ml of Hsp27 solution and reacted for 15 mins at room temperature. Then 1.4 μl 2-mercaptoethanol (final concentration of 20 mM) was added to quench the activity of EDC. Then pK19 was added to the reaction system at an equal molar ratio with Hsp27, and the proteins were allowed to react for 2 h at room temperature. Then Tris was added to the reaction system with a final concentration of 50 mM to quench the reaction. Cross-linking products were analyzed by SDS-PAGE to assess the cross-linking efficiency. Before MS analysis, proteins were precipitated with acetone; the pellet was resuspended in 8 M urea, 100 mM Tris (pH 8.5) and digested with trypsin at room temperature overnight. The resulting peptides were analyzed by online nanoflow liquid chromatography tandem mass spectrometry (LC−MS/MS). And the mass spectrometry data were analyzed by pLink (Yang et al., 2012).

Acknowledgments

We thank staff members of the National Facility for Protein Science in Shanghai, Zhangjiang Laboratory, China for providing technical support and assistance in NMR and BLI data collection. This work was supported by the National Natural Science Foundation (NSF) of China (Grant No. 82188101, 32170683, 31872716 and 32171236), the Science and Technology Commission of Shanghai Municipality (STCSM) (Grant No. 20XD1425000 and 2019SHZDZX02), CAS project for Young Scientists in Basic research (Grant No. YSBR-009), the Shanghai Pilot Program for Basic Research – Chinese Academy of Science, Shanghai Branch (Grant No. CYJ-SHFY-2022-005), the Joint Funds of the National Natural Science Foundation of China (Grant No. U1932204).

Author Contributions

S.Z., J.L., and D.L. designed the project. S.Z., J.L., and Z.L. performed the *in vitro* experiments. Y.Z., A.L., J.L., J.Q., and W.Z. conducted the cellular experiments. All of the authors are involved in analyzing the data and contributed to manuscript discussion and editing. S.Z. and D.L. wrote the manuscript.

Competing Interests

The authors declare no competing interests.

Data and materials availability: All data needed to evaluate the conclusions in the paper are present in the paper and/or the Supplementary Materials. All data generated or analysed during this study are included in the manuscript and supporting file; Source Data files have been provided for Figures 2-7.

REFERENCES

Abisambra, J.F., Blair, L.J., Hill, S.E., Jones, J.R., Kraft, C., Rogers, J., Koren, J., 3rd, Jinwal, U.K., Lawson, L., Johnson, A.G*., et al.* (2010). Phosphorylation dynamics regulate Hsp27-mediated rescue of neuronal plasticity deficits in tau transgenic mice. J Neurosci *30*, 15374-15382.

Alderson, T.R., Roche, J., Gastall, H.Y., Dias, D.M., Pritisanac, I., Ying, J., Bax, A., Benesch, J.L.P., and Baldwin, A.J. (2019). Local unfolding of the HSP27 monomer regulates chaperone activity. Nat Commun *10*, 1068.

Ali, Y.O., Ruan, K., and Zhai, R.G. (2012). NMNAT suppresses tau-induced neurodegeneration by promoting clearance of hyperphosphorylated tau oligomers in a Drosophila model of tauopathy. Hum Mol Genet *21*, 237-250.

Ando, K., Maruko-Otake, A., Ohtake, Y., Hayashishita, M., Sekiya, M., and Iijima, K.M. (2016). Stabilization of Microtubule-Unbound Tau via Tau Phosphorylation at Ser262/356 by Par-1/MARK Contributes to Augmentation of AD-Related Phosphorylation and Abeta42-Induced Tau Toxicity. PLoS Genet *12*, e1005917.

Avila, J. (2006). Tau phosphorylation and aggregation in Alzheimer's disease pathology. FEBS Lett *580*, 2922-2927.

Barghorn, S., Biernat, J., and Mandelkow, E. (2005). Purification of recombinant tau protein and preparation of Alzheimer-paired helical filaments in vitro. Methods in molecular biology (Clifton, NJ) *299*, 35-51.

Baughman, H.E.R., Clouser, A.F., Klevit, R.E., and Nath, A. (2018). HspB1 and Hsc70 chaperones engage distinct tau species and have different inhibitory effects on amyloid formation. J Biol Chem *293*, 2687-2700.

Baughman, H.E.R., Pham, T.T., Adams, C.S., Nath, A., and Klevit, R.E. (2020). Release of a disordered domain enhances HspB1 chaperone activity toward tau. Proc Natl Acad Sci U S A *117*, 2923-2929.

Biernat, J., Gustke, N., Drewes, G., Mandelkow, E.M., and Mandelkow, E. (1993). Phosphorylation of Ser262 strongly reduces binding of tau to microtubules: distinction between PHF-like immunoreactivity and microtubule binding. Neuron *11*, 153-163.

Bjorkdahl, C., Sjogren, M.J., Zhou, X., Concha, H., Avila, J., Winblad, B., and Pei, J.J. (2008). Small heat shock proteins Hsp27 or alphaB-crystallin and the protein components of neurofibrillary tangles: tau and neurofilaments. J Neurosci Res *86*, 1343-1352.

Choi, S., Oh, J.H., Kim, H., Nam, S.H., Shin, J., and Park, J.S. (2015). Protective Effect of Tat PTD-Hsp27 Fusion Protein on Tau Hyperphosphorylation Induced by Okadaic Acid in the Human Neuroblastoma

Cell Line SH-SY5Y. Cell Mol Neurobiol *35*, 1049-1059.

Dickey, C.A., Kamal, A., Lundgren, K., Klosak, N., Bailey, R.M., Dunmore, J., Ash, P., Shoraka, S., Zlatkovic, J., Eckman, C.B.*, et al.* (2007). The high-affinity HSP90-CHIP complex recognizes and selectively degrades phosphorylated tau client proteins. J Clin Invest *117*, 648-658.

Drechsel, D.N., Hyman, A.A., Cobb, M.H., and Kirschner, M.W. (1992). Modulation of the dynamic instability of tubulin assembly by the microtubule-associated protein tau. Mol Biol Cell *3*, 1141-1154.

Drewes, G. (2004). MARKing tau for tangles and toxicity. Trends Biochem Sci *29*, 548-555.

Drewes, G., Ebneth, A., Preuss, U., Mandelkow, E.M., and Mandelkow, E. (1997). MARK, a novel family of protein kinases that phosphorylate microtubule-associated proteins and trigger microtubule disruption. Cell *89*, 297-308.

Drubin, D.G., and Kirschner, M.W. (1986). Tau protein function in living cells. J Cell Biol *103*, 2739-2746.

Dujardin, S., Commins, C., Lathuiliere, A., Beerepoot, P., Fernandes, A.R., Kamath, T.V., De Los Santos, M.B., Klickstein, N., Corjuc, D.L., Corjuc, B.T.*, et al.* (2020). Tau molecular diversity contributes to clinical heterogeneity in Alzheimer's disease. Nat Med *26*, 1256-1263.

F, D., S, G., GW, V., G, Z., J, P., and A, B. (1995). NMRPipe: a multidimensional spectral processing system based on UNIX pipes. Journal of Biomolecular Nmr *6*, 277.

Fischbach, K.F., and Dittrich, A.P.M. (1989). The optic lobe of Drosophila melanogaster. I. A Golgi analysis of wild-type structure. Cell and Tissue Research *258*, 441-475.

Freilich, R., Betegon, M., Tse, E., Mok, S.A., Julien, O., Agard, D.A., Southworth, D.R., Takeuchi, K., and Gestwicki, J.E. (2018). Competing protein-protein interactions regulate binding of Hsp27 to its client protein tau. Nat Commun *9*, 4563.

Goedert, M., Jakes, R., and Vanmechelen, E. (1995). Monoclonal antibody AT8 recognises tau protein phosphorylated at both serine 202 and threonine 205. Neurosci Lett *189*, 167-169.

Gu, G.J., Wu, D., Lund, H., Sunnemark, D., Kvist, A.J., Milner, R., Eckersley, S., Nilsson, L.N., Agerman, K., Landegren, U.*, et al.* (2013). Elevated MARK2-dependent phosphorylation of Tau in Alzheimer's disease. J Alzheimers Dis *33*, 699-713.

Hanger, D.P., Anderton, B.H., and Noble, W. (2009). Tau phosphorylation: the therapeutic challenge for neurodegenerative disease. Trends Mol Med *15*, 112-119.

Hanger, D.P., Betts, J.C., Loviny, T.L., Blackstock, W.P., and Anderton, B.H. (1998). New phosphorylation sites identified in hyperphosphorylated tau (paired helical filament-tau) from Alzheimer's disease brain using nanoelectrospray mass spectrometry. J Neurochem *71*, 2465-2476.

Hanger, D.P., Brion, J.P., Gallo, J.M., Cairns, N.J., Luthert, P.J., and Anderton, B.H. (1991). Tau in Alzheimer's disease and Down's syndrome is insoluble and abnormally phosphorylated. Biochem J *275*

(Pt 1), 99-104.

Hanger, D.P., Byers, H.L., Wray, S., Leung, K.Y., Saxton, M.J., Seereeram, A., Reynolds, C.H., Ward, M.A., and Anderton, B.H. (2007). Novel phosphorylation sites in tau from Alzheimer brain support a role for casein kinase 1 in disease pathogenesis. J Biol Chem *282*, 23645-23654.

Hasegawa, M., Morishima-Kawashima, M., Takio, K., Suzuki, M., Titani, K., and Ihara, Y. (1992). Protein sequence and mass spectrometric analyses of tau in the Alzheimer's disease brain. J Biol Chem *267*, 17047-17054.

Haslbeck, M., Franzmann, T., Weinfurtner, D., and Buchner, J. (2005). Some like it hot: the structure and function of small heat-shock proteins. Nat Struct Mol Biol *12*, 842-846.

He, Z., Guo, J.L., McBride, J.D., Narasimhan, S., Kim, H., Changolkar, L., Zhang, B., Gathagan, R.J., Yue, C., Dengler, C.*, et al.* (2018). Amyloid-beta plaques enhance Alzheimer's brain tau-seeded pathologies by facilitating neuritic plaque tau aggregation. Nat Med *24*, 29-38.

Hu, W., Zhang, X., Tung, Y.C., Xie, S., Liu, F., and Iqbal, K. (2016). Hyperphosphorylation determines both the spread and the morphology of tau pathology. Alzheimers Dement *12*, 1066-1077.

Iijima, K., Gatt, A., and Iijima-Ando, K. (2010). Tau Ser262 phosphorylation is critical for Abeta42-induced tau toxicity in a transgenic Drosophila model of Alzheimer's disease. Hum Mol Genet *19*, 2947-2957.

Jakob, U., Gaestel, M., Engel, K., and Buchner, J. (1993). Small heat shock proteins are molecular chaperones. J Biol Chem *268*, 1517-1520.

Johnson, B.A. (2004). Using NMRView to visualize and analyze the NMR spectra of macromolecules. Methods in molecular biology *278*, 313.

Johnson, G.V., Seubert, P., Cox, T.M., Motter, R., Brown, J.P., and Galasko, D. (1997). The tau protein in human cerebrospinal fluid in Alzheimer's disease consists of proteolytically derived fragments. J Neurochem *68*, 430-433.

Jovcevski, B., Kelly, M.A., Aquilina, J.A., Benesch, J.L.P., and Ecroyd, H. (2017). Evaluating the Effect of Phosphorylation on the Structure and Dynamics of Hsp27 Dimers by Means of Ion Mobility Mass Spectrometry. Anal Chem *89*, 13275-13282.

Jovcevski, B., Kelly, M.A., Rote, A.P., Berg, T., Gastall, H.Y., Benesch, J.L., Aquilina, J.A., and Ecroyd, H. (2015). Phosphomimics destabilize Hsp27 oligomeric assemblies and enhance chaperone activity. Chem Biol *22*, 186-195.

Lambert, H., Charette, S.J., Bernier, A.F., Guimond, A., and Landry, J. (1999). HSP27 multimerization mediated by phosphorylation-sensitive intermolecular interactions at the amino terminus. J Biol Chem *274*, 9378-9385.

Lee, W., Tonelli, M., and Markley, J.L. (2015). NMRFAM-SPARKY: enhanced software for biomolecular NMR spectroscopy. Bioinformatics *31*, 1325.

Liu, Z., Zhang, S., Gu, J., Tong, Y., Li, Y., Gui, X., Long, H., Wang, C., Zhao, C., Lu, J.*, et al.* (2020). Hsp27 chaperones FUS phase separation under the modulation of stress-induced phosphorylation. Nat Struct Mol Biol *27*, 363-372.

Ma, X., Zhu, Y., Lu, J., Xie, J., Li, C., Shin, W.S., Qiang, J., Liu, J., Dou, S., Xiao, Y.*, et al.* (2020). Nicotinamide mononucleotide adenylyltransferase uses its NAD(+) substrate-binding site to chaperone phosphorylated Tau. Elife *9*.

Martin, L., Latypova, X., Wilson, C.M., Magnaudeix, A., Perrin, M.L., Yardin, C., and Terro, F. (2013). Tau protein kinases: involvement in Alzheimer's disease. Ageing Res Rev *12*, 289-309.

McGowan, E., Eriksen, J., and Hutton, M. (2006). A decade of modeling Alzheimer's disease in transgenic mice. Trends Genet *22*, 281-289.

Mok, S.A., Condello, C., Freilich, R., Gillies, A., Arhar, T., Oroz, J., Kadavath, H., Julien, O., Assimon, V.A., Rauch, J.N.*, et al.* (2018). Mapping interactions with the chaperone network reveals factors that protect against tau aggregation. Nat Struct Mol Biol *25*, 384-393.

Morishima-Kawashima, M., Hasegawa, M., Takio, K., Suzuki, M., Yoshida, H., Titani, K., and Ihara, Y. (1995). Proline-directed and non-proline-directed phosphorylation of PHF-tau. J Biol Chem *270*, 823-829.

Petrucelli, L., Dickson, D., Kehoe, K., Taylor, J., Snyder, H., Grover, A., De Lucia, M., McGowan, E., Lewis, J., Prihar, G.*, et al.* (2004). CHIP and Hsp70 regulate tau ubiquitination, degradation and aggregation. Hum Mol Genet *13*, 703-714.

Renkawek, K., Bosman, G.J., and de Jong, W.W. (1994). Expression of small heat-shock protein hsp 27 in reactive gliosis in Alzheimer disease and other types of dementia. Acta Neuropathol *87*, 511-519.

Rogalla, T., Ehrnsperger, M., Preville, X., Kotlyarov, A., Lutsch, G., Ducasse, C., Paul, C., Wieske, M., Arrigo, A.P., Buchner, J.*, et al.* (1999). Regulation of Hsp27 oligomerization, chaperone function, and protective activity against oxidative stress/tumor necrosis factor alpha by phosphorylation. J Biol Chem *274*, 18947-18956.

Rosenqvist, N., Asuni, A.A., Andersson, C.R., Christensen, S., Daechsel, J.A., Egebjerg, J., Falsig, J., Helboe, L., Jul, P., Kartberg, F.*, et al.* (2018). Highly specific and selective anti-pS396-tau antibody C10.2 targets seeding-competent tau. Alzheimers Dement (N Y) *4*, 521-534.

Schwalbe, M., Biernat, J., Bibow, S., Ozenne, V., Jensen, M.R., Kadavath, H., Blackledge, M., Mandelkow, E., and Zweckstetter, M. (2013). Phosphorylation of human Tau protein by microtubule affinity-regulating kinase 2. Biochemistry *52*, 9068-9079.

Schwarz, L., Vollmer, G., and Richter-Landsberg, C. (2010). The Small Heat Shock Protein HSP25/27 (HspB1) Is Abundant in Cultured Astrocytes and Associated with Astrocytic Pathology in Progressive Supranuclear Palsy and Corticobasal Degeneration. Int J Cell Biol *2010*, 717520.

Shimura, H., Miura-Shimura, Y., and Kosik, K.S. (2004). Binding of tau to heat shock protein 27 leads to decreased concentration of hyperphosphorylated tau and enhanced cell survival. J Biol Chem *279*, 17957-17962.

Spillantini, M.G., and Goedert, M. (2013). Tau pathology and neurodegeneration. Lancet Neurol *12*, 609-622.

Wesseling, H., Mair, W., Kumar, M., Schlaffner, C.N., Tang, S., Beerepoot, P., Fatou, B., Guise, A.J., Cheng, L., Takeda, S.*, et al.* (2020). Tau PTM Profiles Identify Patient Heterogeneity and Stages of Alzheimer's Disease. Cell *183*, 1699-1713 e1613.

Wittmann, C.W., Wszolek, M.F., Shulman, J.M., Salvaterra, P.M., Lewis, J., Hutton, M., and Feany, M.B. (2001). Tauopathy in Drosophila: neurodegeneration without neurofibrillary tangles. Science *293*, 711-714.

Xia, Y., Prokop, S., and Giasson, B.I. (2021). "Don't Phos Over Tau": recent developments in clinical biomarkers and therapies targeting tau phosphorylation in Alzheimer's disease and other tauopathies. Mol Neurodegener *16*, 37.

Yang, B., Wu, Y.J., Zhu, M., Fan, S.B., Lin, J., Zhang, K., Li, S., Chi, H., Li, Y.X., Chen, H.F.*, et al.* (2012). Identification of cross-linked peptides from complex samples. Nature methods *9*, 904-906.

Zhang, S., Liu, Y.Q., Jia, C., Lim, Y.J., Feng, G., Xu, E., Long, H., Kimura, Y., Tao, Y., Zhao, C.*, et al.* (2021). Mechanistic basis for receptor-mediated pathological alpha-synuclein fibril cell-to-cell transmission in Parkinson's disease. Proc Natl Acad Sci U S A *118*.

Zhou, G., Ding, Y.H., Xu, D., Na, L., Zhang, E.E., Dong, M.Q., and Tang, C. (2015). Visualizing the Ensemble Structures of Protein Complexes Using Chemical Cross-Linking Coupled with Mass Spectrometry. Biophysics Reports *1*, 127-138.

Figures and Tables

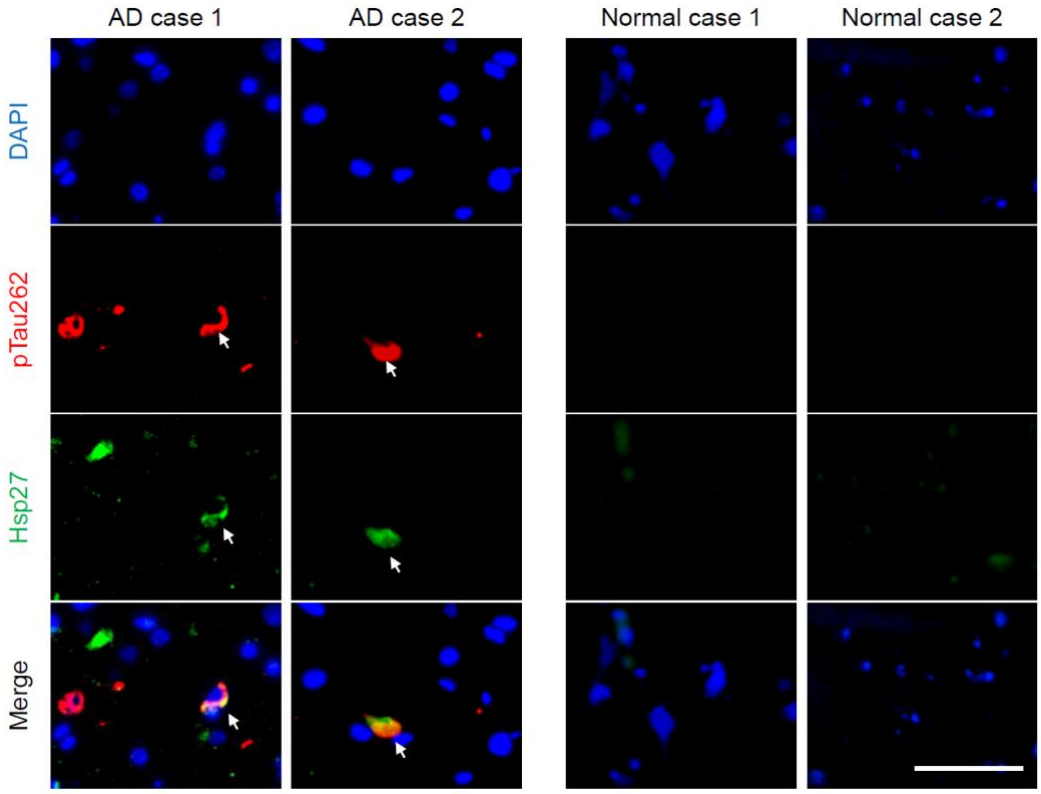

Figure 1 Hsp27 partially co-localizes with pTau aggregates in the brains of AD patients. Representative images of immunofluorescence staining using anti-hyper-phosphorylated Tau at Ser262 and anti-Hsp27 on the brain slices from two AD and two age-matched normal cases. Green, Hsp27; red, pTau^{S262}; blue, DAPI; Scale bar, 50 μm.

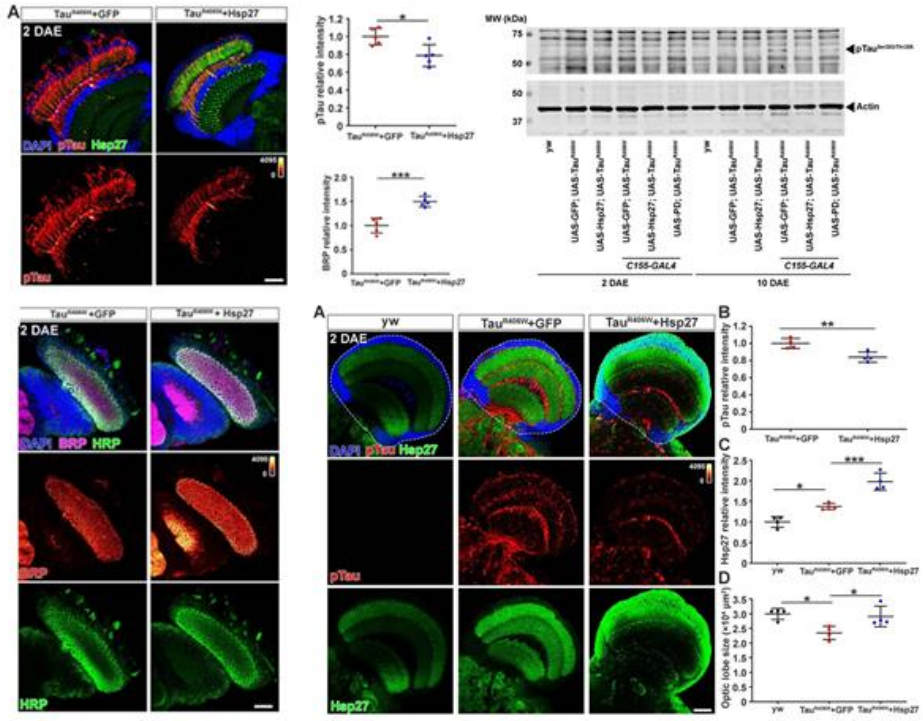

Figure 2 Hsp27 reduces pTau level and protects against pTau-induced synaptopathy in *Drosophila*. (A) Brain lysates of 2 and 10 days after eclosion (DAE) wild-type (WT) flies (lanes 1 and 6), flies expressing human Tau with GFP (lanes 4 and 9), or human Tau with Hsp27 (lanes 5 and 10) in the nervous system were probed with antibodies for disease-associated phospho-tau epitopes S262, Ser202/Thr205 (AT8), and total Tau (5A6). Actin was probed as a loading control. Brain lysates of flies carrying only UAS elements were loaded for control (lanes 2, 3, 7, and 8). (B) Quantification of protein fold changes in (A). The levels of Tau species were normalized to actin. Fold changes were normalized to the Tau+GFP group at 2 DAE. n = 3. (C) Brains of WT flies or flies expressing Tau+GFP or Tau+Hsp27 in the nervous system at 2 DAE were probed for AT8 (heatmap) and Hsp27 (green), and stained with DAPI (blue). Scale bar, 30 μm. (D-F) Quantification of the Hsp27 intensity (D, data normalized to WT), brain optic lobe size (E), and AT8 intensity (F, data normalized to the Tau+GFP group). n = 4. (G) Brain of flies expressing Tau+GFP or Tau+Hsp27 in photoreceptors were probed for AT8, Hsp27, bruchpilot (BRP), and horseradish peroxidase (HRP). Scale bar, 30 μm. (H, I) Quantification of AT8 intensity (H) and BRP intensity (I). Data were normalized to the Tau+GFP group. n = 5. Statistical analyses were performed using one-way ANOVA with Bonferroni's post hoc test (B, D, E) or independent samples t-test (F, H, I). All data are presented as mean ± SD. *P < 0.05, **P < 0.01, ***P < 0.001, ****P < 0.0001.

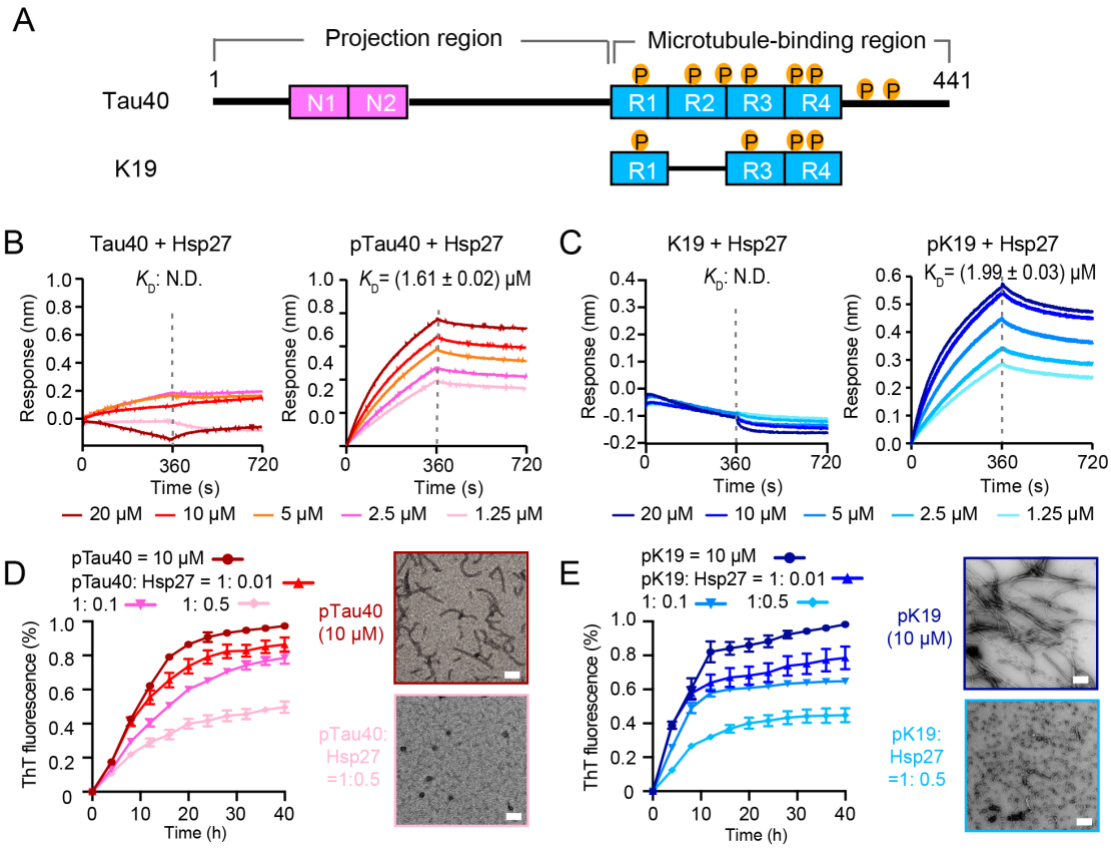

Figure 3 Hsp27 specifically binds MARK2-phosphorylated Tau and prevents its amyloid aggregation. (A) Domain schematic of the longest isoform of Tau (Tau40) and a truncated construct K19. Different isoforms of Tau are characterized by 0, 1, or 2 N-terminal insertions (N1 and N2), and three (R1-R3-R4) or four (R1-4) microtubule-binding repeats. The MARK2-phosphorylated sites are indicated. (B) Binding affinity of Tau40/pTau40 with Hsp27 determined by BLI. The association and dissociation profiles of Tau40/pTau40 to Hsp27 were divided by a vertical dash line. Tau40/pTau40 was fixed to the sensor, and the 5 concentrations of Hsp27 used are indicated. N.D., not detectable. (C) Binding affinity of K19/pK19 with Hsp27 determined by BLI. (D&E) Inhibition of Hsp27 on the amyloid aggregation of 10 μM pTau40 (D)/pK19 (E) revealed by ThT fluorescence kinetic assay (left) and TEM microscopy (right). A gradient concentration of Hsp27 was applied as indicated. The ThT data showed correspond to mean ± SEM, with n = 3. Scale bar in TEM images, 50 nm.

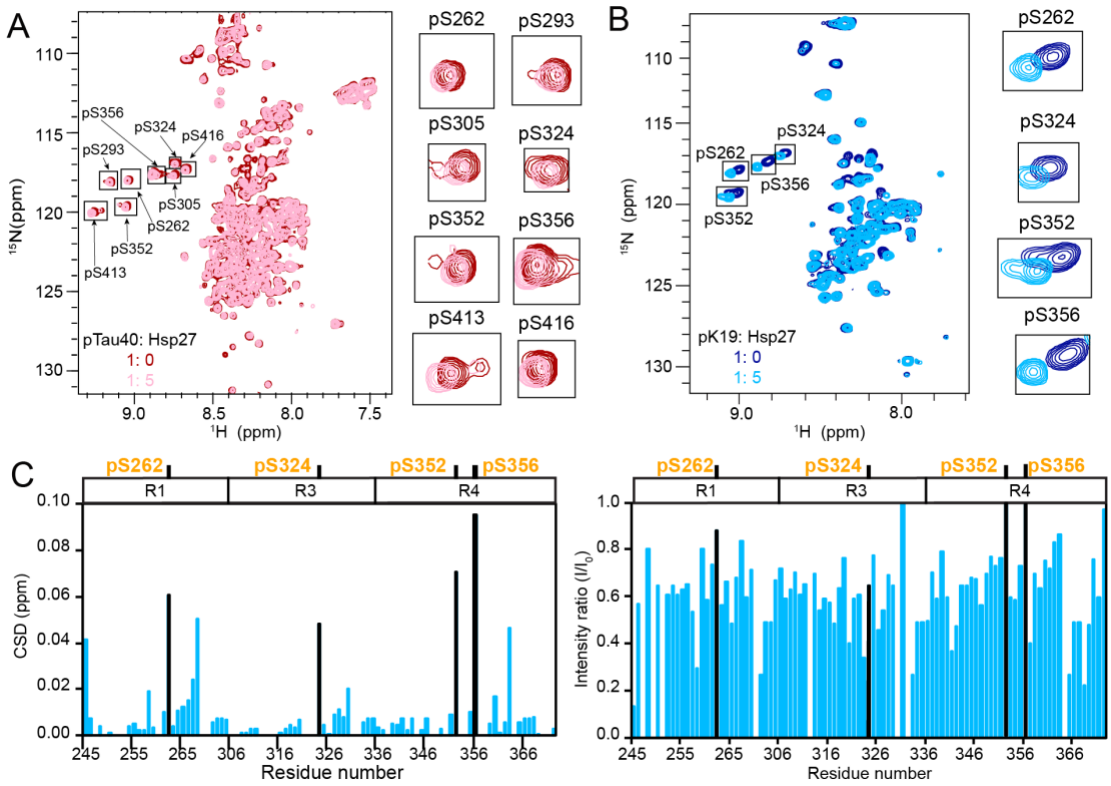

Figure 4 The phosphorylation sites of pTau strongly interact with Hsp27. (A&B) Overlay of the 2D ^{1}H-^{15}N HSQC spectra of 50 μM pTau40 (A) and 50 μM pK19 (B) in the absence and presence of 250 μM Hsp27. Signals of pSer residues are enlarged and labeled on the right. (C) Residue-specific CSDs (left) and intensity changes (right) of pK19 titrated by Hsp27 from (B). The domain organization of pK19 is indicated on top and the data of pSer residues are labeled.

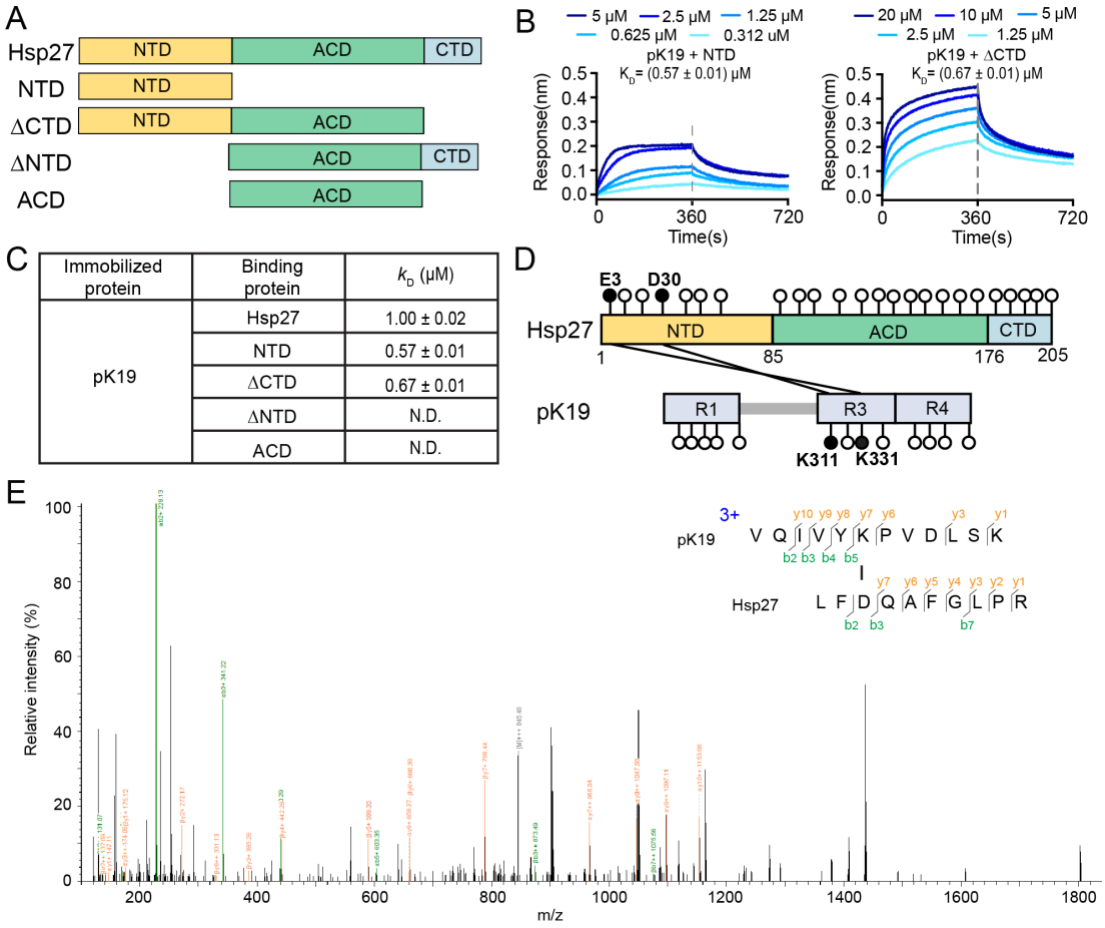

Figure 5 N-terminal domain of Hsp27 is essential in binding with pK19. (A) Domain origination of Hsp27 and the four truncations. (B) Binding affinity of pK19 with NTD and ΔCTD of Hsp27 determined by BLI. The association and dissociation profiles were divided by a vertical dash line. pK19 was fixed to the sensor, and the 5 concentrations of Hsp27 truncations used are indicated. (C) Summary of the binding affinity of pK19 with Hsp27 wild type and truncations. (D) Schematic profile of the cross-linked results of Hsp27 to pK19 using cross-linkers EDC and NHS. All GLU (E) and ASP (D) residues in Hsp27, and all LYS (K) residues in pK19 are indicated by circles, respectively. The two identified crosslinked segments are indicated by two black lines and the corresponding residues are highlighted in black circles and labeled. (E) A representative MS/MS spectrum of trypsin proteinase-generated peptide. The m/z of fragment ions were matched to their theoretical values generated by in silico fragmentation.

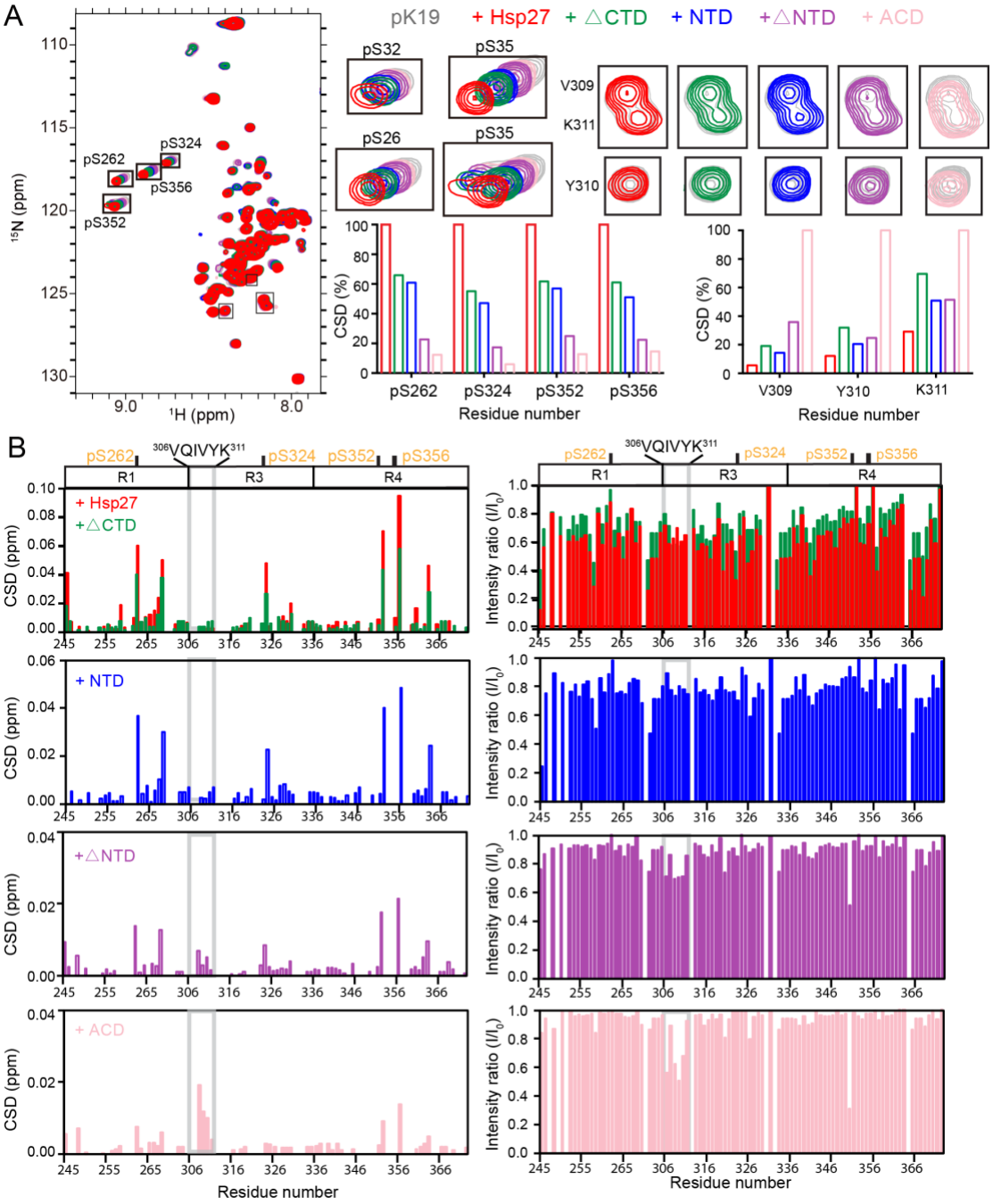

Figure 6 Interaction between pK19 and different domains of Hsp27. (A) Overlay of the 2D ^{1}H-^{15}N HSQC spectra of 50 μM pK19 in the absence and presence of 100 μM Hsp27 variants as indicated. Signals of the four pSer residues and residues V309, Y310, and K311 are labeled and enlarged on the right. Relative CSDs of the four pSer residues and residues V309, Y310, and K311 of pK19 titrated by Hsp27 variants are shown on the right. (B) Residue-specific CSDs (left) and intensity changes (right) of pK19 titrated by Hsp27 variants from (A). Domain organization of pK19 is indicated on top and the pSer residues are indicated. The amyloidogenic ^{306}VQIVYK^{311} region of pK19 was labeled and highlighted by light grey lines.

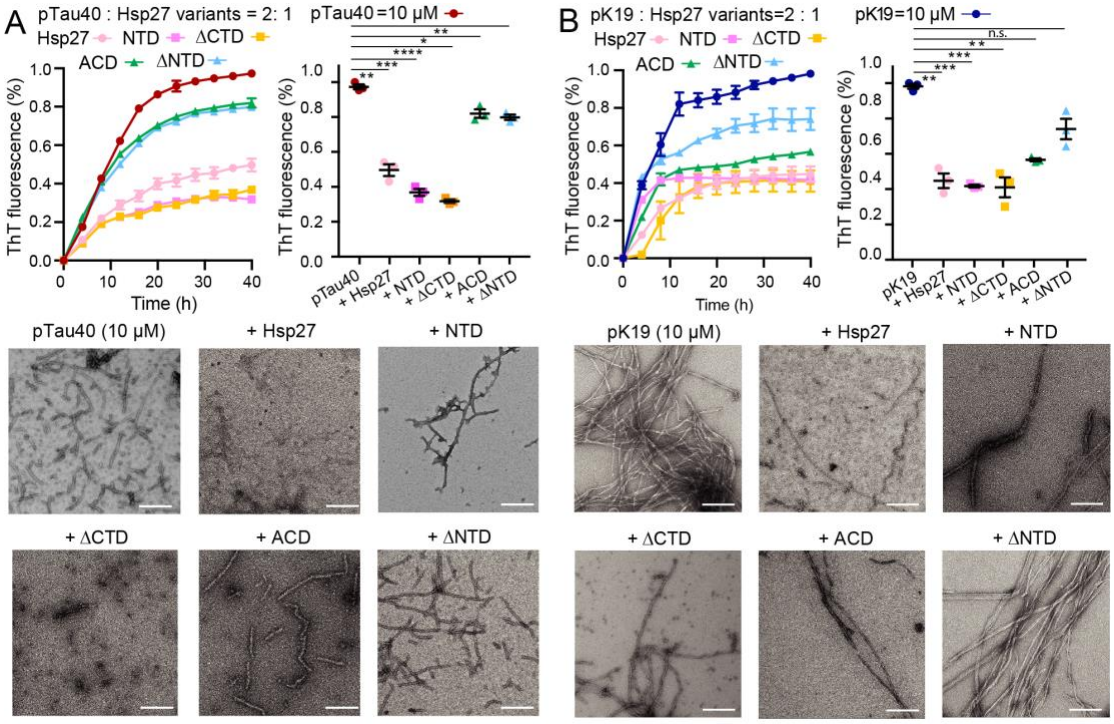

Figure 7 Different domains of Hsp27 play distinctive roles in preventing pTau amyloid aggregation. (A&B) Inhibition of Hsp27 variants on the amyloid aggregation of 10 μM pTau40 (A)/pK19 (B) revealed by ThT fluorescence kinetic assay (top) and TEM microscopy (bottom). The ThT data showed correspond to mean ± s.d., with n = 3 biologically independent samples. Comparison of the inhibitory effect of Hsp27 variants on pTau aggregation at 40-h time point is shown on the right. P values based on two-sided Student's t-test. *P < 0.05, **P < 0.01, ***P < 0.001, ****P < 0.0001, n.s., not significant. Scale bar in TEM images, 200 nm.

Table 1. Summary of the AD patients and age-matched healthy controls.

Cases	Gender	Age	Brain region	Thal Phase (0-3, Aβ plaques)	Braak stage (0-6, Tau)	CERAD (0-3, neuritic plaque)
AD case 1	F	76	Frontal cortex	3	3	3
AD case 2	F	74	Frontal cortex	3	3	3
Normal case 1	M	77	Frontal cortex	0	0	0
Normal case 2	F	70	Frontal cortex	0	0	0

Table 2. Cross-linked peptides between pK19 and Hsp27. The crosslinked residues are bold and underlined in the sequences.

	Peptide sequence (Hsp27-pK19)	Score 1	Score 2	Score 3
1	LF**D**QAFGLPR - VQIVY**K**PVDLSK	2.56246E-11	3.17803E-09	1.21049E-06
2	GSEFENLYFQGMT**E**R-CGSLGNIHH**K**PGGGQVEVK	5.05514E-09	1.37169E-06	9.56423E-07

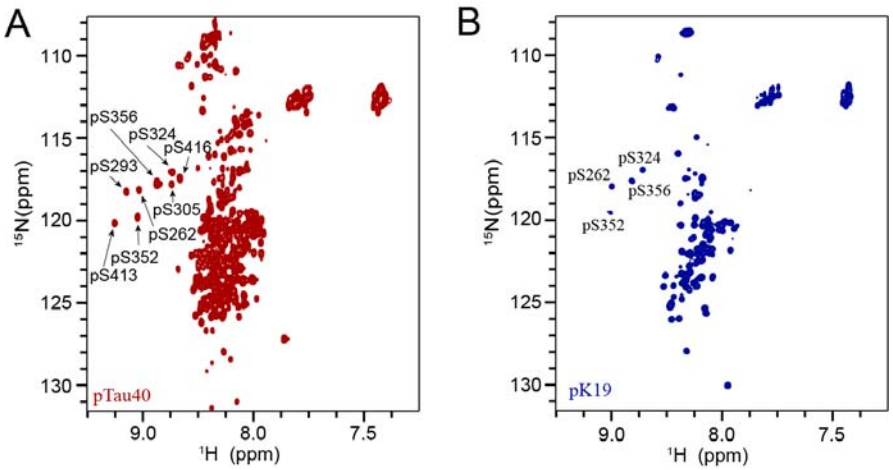

Supplementary Fig. 1 2D ^{1}H-^{15}N HSQC spectra of pTau40 (A) and pK19 (B) collected at 298 K on a Bruker Avance 900 MHz spectrometer. 100 μM pTau40 and pK19 were in the NMR buffer of 50 mM Na_2HPO_4, 50 mM NaCl and 10% (v/v) D_2O at pH 7.0. The eight and four phosphorylated residues are labeled in the spectra of pTau40 and pK19, respectively.

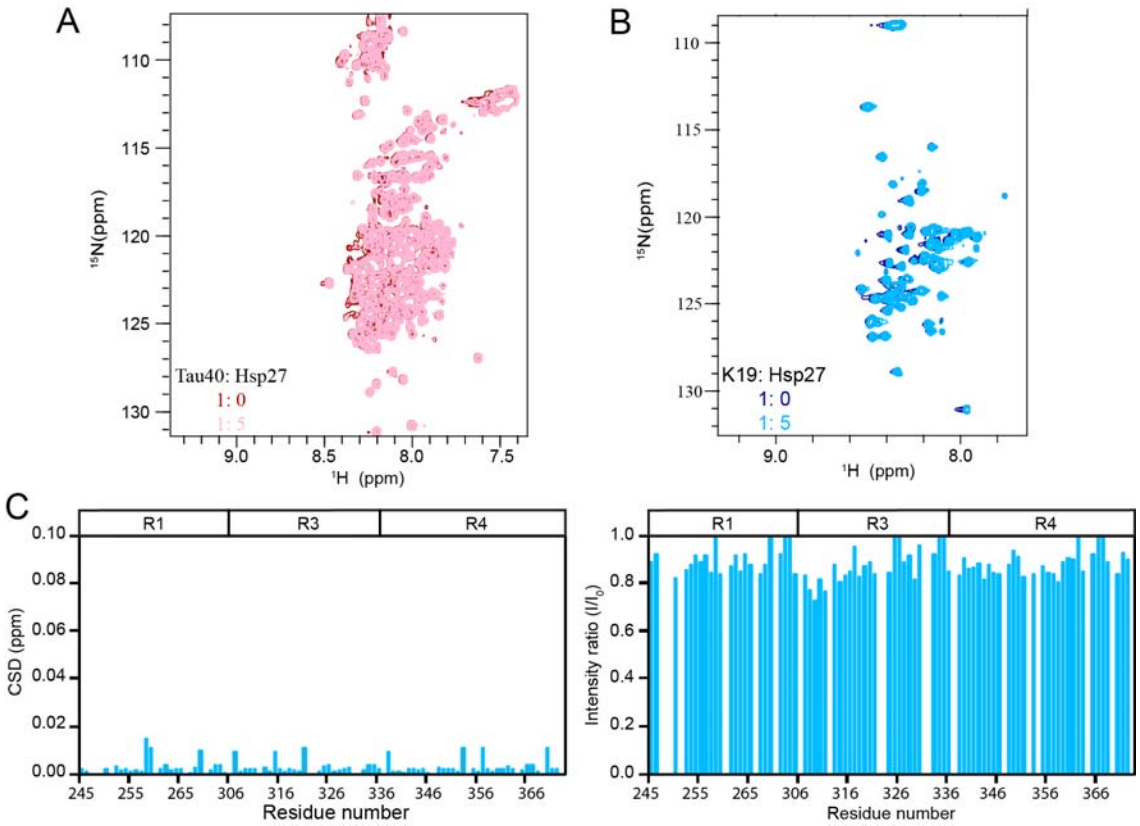

Supplementary Fig. 2 Hsp27 interacts very weakly with unphosphorylated Tau. (A&B) Overlay of the 2D ^{1}H-^{15}N HSQC spectra of 50 µM Tau40 (A) and 50 µM K19 (B) in the absence and presence of 250 µM Hsp27. (C) Residue-specific chemical shift changes (left) and intensity changes (right) of k19 titrated by Hsp27 from (B). The domain organization of K19 is indicated on top.

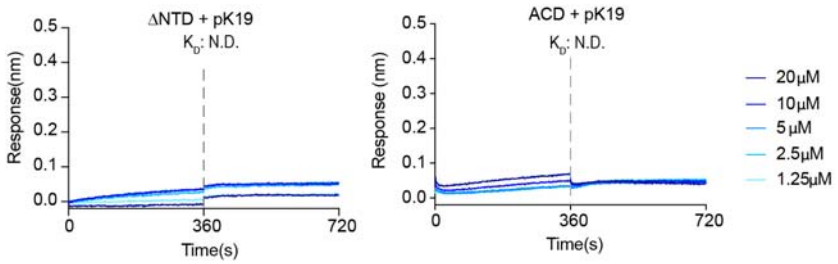

Supplementary Fig. 3 Binding affinity of pK19 with ΔNTD and ACD of Hsp27 determined by BLI. The association and dissociation profiles were divided by a vertical dash line. pK19 was fixed to the sensor, and the 5 concentrations of Hsp27 truncations used are indicated. N.D., not detectable.